chemistry

MDPI

Article

Structural Diversity of Lithium Oligo-α-Pyridylamides

Arsen Raza [1,2], Adele Mucci [1], Alessio Nicolini [1] and Andrea Cornia [1,*]

[1] Department of Chemical and Geological Sciences and INSTM Research Unit, University of Modena and Reggio Emilia, Via G. Campi 103, 41125 Modena, Italy; arsen.raza@unifi.it (A.R.); adele.mucci@unimore.it (A.M.); alessio.nicolini@unimore.it (A.N.)

[2] Department of Industrial Engineering and INSTM Research Unit, University of Florence, Via S. Marta 3, 50139 Florence, Italy

* Correspondence: acornia@unimore.it; Tel.: +39-059-205-8645

Abstract: Lithium oligo-α-pyridylamides are useful intermediates in coordination chemistry. Upon *trans-metalation* they have afforded a variety of extended metal atom chains (EMACs), which are currently investigated as molecular wires and single-molecule magnets. However, structural information on this class of compounds is scarce. Two trilithium salts of a new, sterically encumbered oligo-α-pyridylamido ligand were isolated in crystalline form and structurally characterized in the solid state and in solution. Lithiation of N^2-(trimethylsilyl)-N^6-{6-[(trimethylsilyl)amino]pyridin-2-yl}pyridine-2,6-diamine (H_3L) with *n*-BuLi in thf yielded dimeric adduct $[Li_6L_2(thf)_6]$ (**1**), which was crystallized from *n*-hexane/thf as **1**·C_6H_{14}. Crystals of a tetra-thf solvate with formula $[Li_6L_2(thf)_4]$ (**2**) were also obtained. The compounds feature two twisted L^{3-} ligands exhibiting a *cis-cis* conformation and whose five nitrogen donors are all engaged in metal coordination. The six Li^+ ions per molecule display coordination numbers ranging from 3 to 5. Compound **1**·C_6H_{14} was investigated by multinuclear 1D and 2D NMR spectroscopy, including ^{1}H DOSY experiments, which indicated retention of the dimeric structure in benzene-d_6 solution. To the best of our knowledge, **1** and **2** are the longest-chain lithium oligo-α-pyridylamides structurally authenticated so far, thereby qualifying as appealing intermediates to access high-nuclearity EMACs by *trans-metalation*.

Keywords: lithium amides; X-ray diffraction; NMR spectroscopy; diffusion ordered spectroscopy

check for updates

Citation: Raza, A.; Mucci, A.; Nicolini, A.; Cornia, A. Structural Diversity of Lithium Oligo-α-Pyridylamides. *Chemistry* **2022**, *4*, 520–534. https://doi.org/10.3390/chemistry4020037

Academic Editor: Bartolo Gabriele

Received: 15 April 2022
Accepted: 22 May 2022
Published: 25 May 2022

1. Introduction

N-anionic ligands such as amidinates, guanidinates, 2-aminopyridinates, and their combinations are important synthetic building blocks in coordination chemistry [1–3]. A vast series of extended metal atom chain (EMAC) compounds [4] containing up to 11 metal ions [5] were assembled using arrays of lined-up N donors as those provided by oligo-α-pyridylamido ligands in their all-*cis* conformation [6]. These wire-like structures often contain metal-metal bonds, which may give rise to unusual electrical or magnetic properties. For instance, the doubly-deprotonated form of proligand H_2L' in Figure 1 was used to stabilize a linear triiron(II) species featuring a Fe-Fe separation of only 2.44 Å and an $S = 6$ ground state [7]. More recently, a structurally similar complex containing 2-pyridyl-substituted formamidinato ligands, first reported in 1998 by Cotton et al. [8], was also shown to have $S = 6$ and to exhibit single-molecule magnet properties despite the longer Fe-Fe distance of 2.78 Å [9].

These molecular compounds are most often prepared by one of two possible routes [10–12]: (a) *direct metalation*, which implies reacting the organic proligand with a transition-metal halide and an exogenous base (e.g., *t*-BuONa or *t*-BuOK) in refluxing naphthalene (Hurley-Robinson-Peng's method) [13,14]; (b) *trans-metalation* between a lithium salt of the organic ligand and a transition-metal halide (Cotton's method) [15]; the lithium salt is typically prepared in situ by treating the organic proligand with MeLi [8,9,15] or *n*-BuLi [7] in thf at low temperature and is not isolated. Other routes have been proposed, such as: (c) the use

of an organometallic precursor (e.g., $[Fe_2(Mes)_4]$, HMes = mesitylene) that provides the required basic equivalents while acting as a metal source [16,17]; (d) reaction of a precursor metal complex of the proligand with MeLi [12]. More sophisticated methods were devised to access heterometallic variants [11,18].

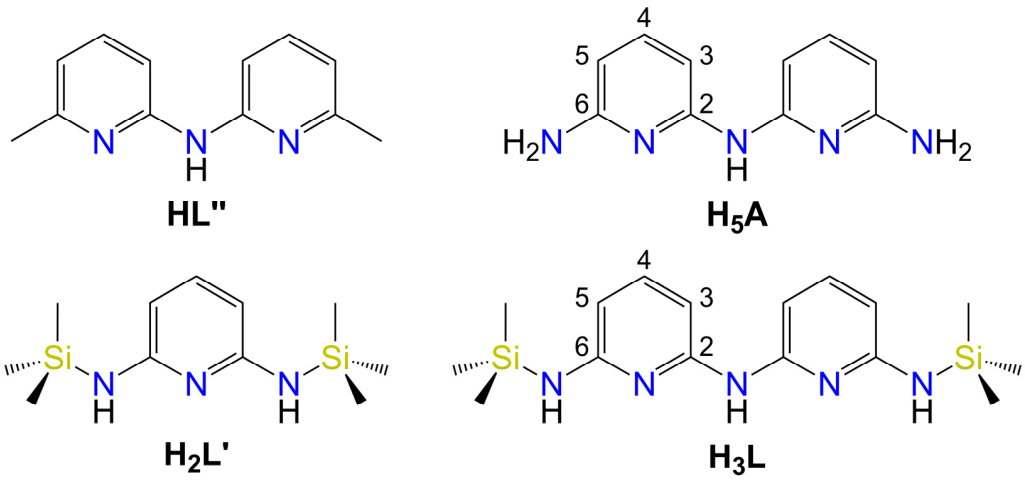

Figure 1. Molecular structures of HL″, H_5A, H_2L', and H_3L.

In spite of their relevance as intermediates in *trans-metalation* reactions, lithium oligo-α-pyridylamides have been structurally characterized only rarely and the available information is limited to the shortest members of the series. When prepared from toluene/hexane, the lithium salt of HL″ in Figure 1 is tetrameric in the solid state ($[Li_4L''_4]$) and contains pairs of μ_4- and μ_2-L''^{-} ligands [2]. Two lithium salts of H_2L' (Figure 1) were prepared in crystalline form from hexane(s)/thf and structurally authenticated as $[Li_4(HL')_2L'(thf)_2]$ [19] and $[Li_4L'_2(thf)_4]$ [7]. The L'^{2-} and HL'^{-} anions in these complexes act as μ_4- and μ_3-ligands, respectively. A thf-free form was also synthesized from hexane [20]. Lithium 2,2′-dipyridylamide (dpa^{-}) crystallized from 2-MeTHF/hexane is dimeric and has formula $[Li_2(dpa)_2(2\text{-MeTHF})_2]$, with two μ_2-dpa^{-} ligands [21].

In this work we have prepared the higher homologue of sterically encumbered H_2L', namely proligand H_3L in Figure 1, and its trilithium salt. When crystallized from *n*-hexane/thf, the latter compound is dimeric in the solid state and has formula $[Li_6L_2(thf)_6]\cdot C_6H_{14}$ (**1**·C_6H_{14}). A tetra-thf solvate $[Li_6L_2(thf)_4]$ (**2**) was also structurally authenticated, which showed a massive effect of thf coordination on the geometry of the hexalithium core. In both compounds the two oligo-α-pyridylamido ligands are twisted from each other and adopt a *cis-cis* conformation, with all their N donors engaged in metal coordination. A multinuclear NMR spectroscopy investigation on **1**·C_6H_{14} indicated retention of its dimeric structure in benzene-d_6 solution. To the best of our knowledge, **1** and **2** are the longest-chain lithium oligo-α-pyridylamides structurally authenticated so far. Thus, they qualify as appealing intermediates to access high-nuclearity EMACs by *trans-metalation*.

2. Materials and Methods

General procedures. All synthetic operations involving air- or water-sensitive compounds were conducted under N_2 using a Schlenk line or inside an MBraun UniLAB glove-box with < 1 ppm of O_2 and H_2O. The glove-box is equipped with a Julabo FT-902 cold-finger cryostat and an *n*-heptane cooling bath for low-temperature reactions. Solvents and reagents were purified as follows (DPK = sodium diphenylketyl solution; 3FPT = three freeze-pump-thaw cycles; MS = activated 4A molecular sieves) [22]. Tetrahydrofuran (thf) was pre-dried over KOH (24 h), distilled, re-distilled from DPK under N_2, degassed by 3FPT, and stored on MS. *n*-Hexane was degassed by 3FPT and stored on MS. Triethylamine (Et_3N) was dried on CaH_2 overnight, distilled, and stored on MS. Ethanol was stored on MS before use. Black, commercial 2,6-diaminopyridine (dap) was purified by

sublimation to give a perfectly white crystalline solid (Mp 120.5–121.0 °C; lit.: 120–121 °C from ligroin [23]). Benzene-d_6 was degassed by 3FPT and stored on MS. Trimethylsilyl chloride (TMSCl) was treated with CaH_2 (24 h) and obtained under N_2 flow. All the other chemicals were used as received. Commercial *n*-BuLi solution (1.6 M in hexanes) was titrated before use [24].

A solution of HCl in Et_2O was prepared by adding 37% (*w*/*w*) hydrochloric acid (8.3 mL, 0.10 mol) to Et_2O (39 mL), followed by powdered $MgSO_4$ (21.6 g) in small portions. After stirring for several hours, the liquid phase was decanted away, the solid washed with Et_2O (3 × 5 mL), and the volume of the combined organic phases adjusted to 50 mL. The solution was titrated with 0.1 M NaOH and bromothymol blue indicator shortly before use (concentrations usually ranged from 0.65 to 0.85 M) [25].

Elemental analysis was carried out with a Flash 2000 automatic analyzer from Thermo Fisher Scientific (Waltham, WA, USA).

NMR spectra were collected on AVANCE400 (operating at 400.13 MHz for ^{1}H) and AVANCE III HD (operating at 600.13, 233.23, 150.90, and 60.85 MHz for ^{1}H, ^{7}Li, ^{13}C, and ^{15}N, respectively) FT-NMR spectrometers from Bruker Biospin. The air-sensitive samples were prepared directly in the glove-box using 5 mm NMR tubes equipped with Young valves. ^{1}H and ^{13}C spectra were calibrated setting the solvent residual proton signals in dimethyl sulfoxide-d_6 and benzene-d_6 at 2.50 and 7.16 ppm, respectively, and the solvent ^{13}C signal in benzene-d_6 at 128.06 ppm [26]. Heteronuclear spectra were referenced to a 1 M solution of LiCl in D_2O (^{7}Li) or to liquid ammonia (^{15}N). The following abbreviations are used in reporting NMR data: s = singlet, d = doublet, t = triplet, m = multiplet, br = broad, and vbr = very broad. The spectra were analyzed and plotted with Bruker TopSpin 4.0.9 software. 2D NMR experiments were carried out using standard pulse sequences (Bruker library): cosygpqf (^{1}H-^{1}H COSY), hsqcedetgpsp.3 (^{1}H-^{13}C HSQCed), roesyph (^{1}H-^{1}H ROESY, 250 ms mixing time), hmbcetgpl3nd (^{1}H-^{13}C HMBC, 50 ms evolution time), and hmbcgpndqf (^{1}H-^{15}N HMBC, 200 ms evolution time).

The ^{1}H diffusion-ordered experiment (^{1}H DOSY) was run at 400.13 MHz and 298 K in benzene-d_6, with a ledbpgp2s sequence using bipolar gradient pulses [27], a big delta of 60 ms and a little delta of 2 ms. The signal decay was fitted with a double exponential function with Bruker Dynamic Center software, to take into account the partial overlapping of some signals. The diffusion coefficient of the residual proton signal of benzene-d_6 was used to calculate the normalized diffusion coefficients $D_{x,norm}$ and to estimate the molecular weight (*MW*) of **1** based on the external calibration curves (ECCs) for benzene-d_6 solutions proposed by Bachmann et al. [28]. Parameters in the equation $\log MW = (\log D_{x,norm} - \log K)/\alpha$ are: $\log K = -7.58$ and $\alpha = -0.572$ for merged ECC (ECC_{merge}); $\log K = -7.47$ and $\alpha = -0.622$ for molecules diffusing as "dissipated spheres and ellipsoids" (ECC_{DSE}), a model that proved most successful for organometallics [28,29].

IR spectra were measured in ATR mode on a JASCO 4700 FT-IR spectrometer between 400 and 4000 cm^{-1} with 2 cm^{-1} resolution. The following abbreviations are used in reporting IR data: s = strong, m = medium, and w = weak.

X-ray Crystallography. All structures were analyzed with a four-circle Bruker-Nonius X8APEX diffractometer equipped with Mo-Kα radiation (λ = 0.71073 Å) and a Kryoflex liquid N_2 cryostat. A needle-like colorless crystal of β-H_5A was fixed on a glass fiber with epoxy resin for data collection at room temperature. Colorless crystals of **1**·C_6H_{14} (prisms) and **2** (blocks) were removed from the mother liquor under N_2 atmosphere, immediately soaked in NVH immersion oil (Jena Bioscience) and mounted on top of a glass capillary and on a 200 µm MiTeGen MicroLoop^{TM}, respectively, for data collection at 115(2) K. Data collection and reduction were carried out using APEX2 v1.0-22 [30] and SAINT v7.06A [30] software, respectively, while a multi-scan absorption correction was applied with SADABS v2.10 [30]. The structures were solved by direct methods using the SIR92 program [31]. Full matrix least-squares refinement on F_o^2 was performed with the SHELXL-2018/3 program [32] implemented in the WINGX v2020.2 suite [33]. Unless otherwise noted, all nonhydrogen atoms were refined anisotropically, while hydrogen atoms were

set in idealized positions and treated as riding contributors with isotropic displacement parameters tied to 1.5 or 1.2 times those of the parent atoms for CH_3 and other hydrogens, respectively. A rotating group refinement (AFIX 137) was adopted for trimethylsilyl CH_3 groups. Specific refinement details for each structure are reported hereafter.

The crystals of β-H_5A are monoclinic, with systematic absences clearly pointing to space groups *Cc* or *C*2/*c*. Structure solution was possible in both space groups, but refinement could be satisfactorily carried out only in *Cc*. The asymmetric unit contains two independent molecules (Z = 8). To increase the data/parameter ratio, coordinates were refined only for NH- and NH_2-type hydrogen atoms, with a single U_{iso} parameter for each type. The experimental data did not support the determination of the absolute structure.

The crystals of **1**·C_6H_{14} are orthorhombic (space group *Pbcn*) and the asymmetric unit contains half molecule of **1** which develops around a twofold axis (Z = 4) and consequently has crystallographically imposed C_2 symmetry. One thf ligand is disordered over two positions (0.563(8):0.437(8)) and was refined with restraints on geometry (SAME) and anisotropic displacement parameters (RIGU) [34]. A half-occupancy *n*-hexane molecule disordered around a twofold axis is also present in the asymmetric unit. It is further split over two positions (0.258(4):0.242(4)) and was refined isotropically with restraints on geometry (DFIX, SAME) and constraints on anisotropic displacement parameters (EADP).

The crystals of **2** are triclinic (space group $P\bar{1}$) and the asymmetric unit contains two distinct molecules (Z = 4): Li1-Li6 (mol1) and Li7-Li12 (mol2). Two thf ligands in mol2 are split over two positions with 0.637(10):0.363(10) and 0.653(11):0.347(11) occupancies, respectively. They were refined with restraints on geometry (SAME) and constraints or restraints on anisotropic displacement parameters (EADP, RIGU) [34].

Graphics utilized ORTEP-3 for Windows v2014.1 [33] and POV-Ray for Windows v3.7 [35].

CCDC 2165612-2165614 contain the supplementary crystallographic data for this paper. These data can be obtained free of charge from The Cambridge Crystallographic Data Centre via www.ccdc.cam.ac.uk/structures (accessed on 10 April 2022), or by emailing data_request@ccdc.cam.ac.uk, or by contacting The Cambridge Crystallographic Data Centre, 12 Union Road, Cambridge CB2 1EZ, UK; fax: +44 1223 336033.

X-ray Powder Diffraction. X-ray powder diffraction data were acquired on a Panalytical X'Pert PRO diffractometer (θ/θ geometry, Cu-Kα radiation) equipped with an X-celerator detector. The scans were collected for 2θ = 5–120° in steps of 0.017° at a rate of 210 s per step. Powder patterns were simulated with Mercury 2021.1.0 [36] using a full-width-at-half-maximum of 0.12° in 2θ.

Synthesis of 2,6-diaminopyridine monohydrochloride (dap·HCl). 2,6-Diaminopyridine (1.51 g, 13.8 mmol) was solubilized in hot EtOH (7 mL) to give a clear, light-yellow solution. After cooling down to room temperature, stoichiometric ethereal HCl (0.65 M) was added dropwise until slightly acidic pH (ca. 21.3 mL, 14 mmol). The biphasic system so obtained became homogeneous upon further addition of EtOH (4 mL). The solvent was removed under vacuum to give a light brown solid (1.94 g, 96%). Mp 82.1–83.3 °C (lit.: 81–83 °C from ethanol [37,38]). Elemental analysis calcd (%) for $C_5H_7N_3$·HCl·H_2O: C 36.71, H 6.16, N 25.68; found: C 36.68, H 6.10, N 26.19. ^{1}H NMR ($(CD_3)_2SO$, 400.13 MHz, 298 K): δ = 5.87 (d, $^3J_{H\text{-}H}$ = 8.3 Hz, 2H, $H^{3,5}$), 7.25 (s, br, 4H, NH_2), 7.47 (t, $^3J_{H\text{-}H}$ = 8.3 Hz, 1H, H^4), 12.83 ppm (s, br, 1H, N^+-H). Mibu et al. reported very close ^{1}H NMR data [39]. The spectrum is clearly indicative of protonation on the pyridine ring, consistent with the solid-state structure of dap·HCl·H_2O determined by Schrage et al. [40].

Synthesis of N^2-(6-aminopyridin-2-yl)pyridine-2,6-diamine (H_5A). 2,6-Diaminopyridine (3.50 g, 32.1 mmol) and 2,6-diaminopyridine monohydrochloride (4.68 g, 32.1 mmol) were introduced in a Schlenk flask kept under N_2 flow. The mixture was heated to an internal temperature of 190 °C in a silicone oil bath, whereupon a lively evolution of NH_3 was observed. The course of the reaction was followed by ^{1}H NMR spectroscopy in dimethyl sulfoxide-d_6 and by TLC (silica gel, 10 mL CH_2Cl_2/EtOH 9:1 v/v + 2 drops 30% aqueous NH_3; r.f. = 0.59 for dap and 0.65 for H_5A). After 57 h the initially liquid reaction mixture

had turned into a black hard solid. The ^{1}H NMR spectrum ($(CD_3)_2SO$, 400.13 MHz, 298 K) showed a dominant pattern of resonances assigned to $H_5A{\cdot}HCl$: δ = 6.17 (d, $^3J_{H\text{-}H}$ = 8.2 Hz, 2H, H^3 or H^5), 6.22 (d, $^3J_{H\text{-}H}$ = 8.2 Hz, 2H, H^3 or H^5), 7.55 (t, $^3J_{H\text{-}H}$ = 8.2 Hz, 2H, H^4), 7.59 (s, vbr, 4H, NH_2), 11.05 (s, br, 1H, NH), 15.64 ppm (s, br, 1H, N^+-H). A weaker set of signals from dap·HCl (see above) was also detected, indicating an approximately 3:1 molar ratio between the two species. The reaction was prosecuted for additional 12 h, then the solid mass was cooled down to room temperature, finely ground and subject to a first extraction with hot EtOH (200 mL) under stirring to remove the reactants. The solid was collected by filtration (G3) and subject to further prolonged extraction with EtOH (200 mL) in a Soxhlet apparatus. Removal of the solvent under vacuum gave crude $H_5A{\cdot}HCl$ as a brown powder (4.13 g). A portion of this crude monohydrochloride (3.12 g) was refluxed with EtOH (920 mL) for 2 h. A small amount of insoluble material was removed by filtration on a G3 glass frit, which was washed with hot EtOH (2 × 70 mL). The combined ethanolic solutions were decolorized by boiling with charcoal (~2 g) for 30 min and filtered on Celite. Complete evaporation of the solvent under vacuum afforded purified $H_5A{\cdot}HCl$ as an off-white powder (2.48 g). This monohydrochloride (2.41 g, 10.1 mmol) was dissolved into the minimum amount of boiling water (40 mL) under N_2 flux and treated dropwise and under vigorous stirring with a solution of NaOH (0.422 g, 10.6 mmol) in water (2 mL). The free amine started to precipitate toward the end of the addition and crystallization was completed by slow cooling. The product was collected by filtration, washed with ice water (2 × 2 mL) and thoroughly dried under vacuum until constant weight (1.86 g). An additional crop of crystals was obtained by decolorization of the first extract with charcoal, complete removal of the solvent under vacuum, trituration of the solid with water to dissolve the reactants, and liberation of the amine by addition of stoichiometric NaOH to a hot water solution (0.45 g). The overall yield of crystalline H_5A was 46%. Mp 174.5–175.0 °C (lit.: 172–173 °C from 50% ethanol [38]; 177–178 °C [41]). Elemental analysis calcd (%) for $C_{10}H_{11}N_5$: C 59.69, H 5.51, N 34.80; found: C 59.11, H 5.30, N 34.38. ^{1}H NMR ($(CD_3)_2SO$, 400.13 MHz, 298 K): δ = 5.54 (s, br, 4H, NH_2), 5.90 (d, $^3J_{H\text{-}H}$ = 7.8 Hz, 2H, H^5), 6.87 (d, $^3J_{H\text{-}H}$ = 7.9 Hz, 2H, H^3), 7.19 (t, $^3J_{H\text{-}H}$ = 7.8 Hz, 2H, H^4), 8.47 ppm (s, br, 1H, NH). Schrage et al. [40] and Lemport et al. [41] reported very close ^{1}H NMR data. IR (ATR): $\tilde{\nu}_{max}$ = 3454 (w), 3349 (w), 3283 (w), 3154 (w), 1610 (m), 1592 (m), 1557 (m), 1527 (m), 1440 (s), 1383 (m), 1353 (m), 1286 (m), 1262 (m), 1158 (m), 1112 (m), 1069 (m), 983 (w), 979 (w), 966 (w), 783 (m), 771 (m), 723 (w), 682 (w), 631 (w), 613 cm^{-1} (w).

Synthesis of N^2-(trimethylsilyl)-N^6-{6-[(trimethylsilyl)amino]pyridin-2-yl}pyridine-2,6-diamine (H_3L). H_5A (1.86 g, 9.24 mmol), thf (37 mL), and triethylamine (2.70 mL, 19.4 mmol) were introduced in a Schlenk flask kept under N_2 flow. Finally, TMSCl (2.45 mL, 19.3 mmol) was added. After 24 h of stirring at room temperature, the solvent was completely removed under vacuum and the residue extracted with *n*-hexane (40 mL) for 2 h. The off-white solid (Et_3NHCl) was removed by filtration (G4) and washed with additional *n*-hexane (10 mL). The solvent was completely removed under vacuum from the combined organic phases to give H_3L as a yellow-orange resinous solid (2.51 g, 79%). Elemental analysis calcd (%) for $C_{16}H_{27}N_5Si_2$: C 55.61, H 7.87, N 20.26; found: C 55.77, H 7.84, N 20.47. ^{1}H NMR (C_6D_6, 600.13 MHz, 298 K): δ = 0.27 (s, 18H, $(CH_3)_3Si$), 3.65 (s, br, 2H, NHSi), 5.74 (d, $^3J_{H\text{-}H}$ = 7.8 Hz, 2H, H^5), 6.72 (d, $^3J_{H\text{-}H}$ = 7.9 Hz, 2H, H^3), 6.82 (s, br, 1H, NH), 7.12 ppm (t, $^3J_{H\text{-}H}$ = 7.8 Hz, 2H, H^4). ^{13}C NMR (C_6D_6, 150.90 MHz, 298 K): δ = 0.25 ($(CH_3)_3Si$), 100.60 (C^3 or C^5), 102.09 (C^3 or C^5), 138.88 (C^4), 153.48 (C^2 or C^6), 159.16 ppm (C^2 or C^6). The product must be stored in a moisture-free environment (preferably in a glove-box) to avoid partial desilylation, which is signaled by the appearance of extra doublets in the aromatic region and of additional peaks in the trimethylsilyl region.

*Synthesis of $[Li_6L_2(thf)_6]{\cdot}C_6H_{14}$ (**1**$\cdot C_6H_{14}$).* In a glove-box, H_3L (2.51 g, 7.26 mmol) was solubilized in thf (13 mL) to give a clear yellow-orange solution which was cooled down to −40 °C. *n*-BuLi (1.54 M, 14.8 mL, 22.8 mmol) was added dropwise under stirring, whereupon the solution turned to an orange color. After warming up to room temperature and stirring overnight, the solvent was completely evaporated under vacuum to yield

the crude lithium salt as a yellow solid (4.39 g). A 0.141 g portion of this crude product was dissolved in the minimum volume of *n*-hexane/thf 10:1 *v*/*v* (ca. 0.7 mL). The orange solution so obtained was introduced in a glass ampoule, which was extracted from the glove-box, flame sealed, and cooled down to −20 °C for several days. The ampoule was rapidly re-introduced in the glove-box and cooled down to −30 °C. The mother liquor was decanted away from colorless crystalline **1**·C_6H_{14}, which was washed with the minimum amount of cold *n*-hexane and finally dried under mild vacuum (0.0973 g, 67%). Elemental analysis calcd (%) for $C_{56}H_{96}Li_6N_{10}O_6Si_4$ (**1**): C 58.01, H 8.35, N 12.08; found on crystals further dried under vacuum: C 57.96, H 8.73, N 11.68. ^{1}H NMR (C_6D_6, 600.13 MHz, 298 K): δ = 0.50 (s, 36H, $(CH_3)_3Si$), 0.89 (t, 6H, CH_3 $_{n\text{-hexane}}$), 1.23 (m, 4H, $CH_2CH_2CH_3$ $_{n\text{-hexane}}$), 1.27 (m, 4H, CH_2CH_3 $_{n\text{-hexane}}$), 1.27 (m, 24H, CH_2CH_2O $_{thf}$), 3.36 (m, 24H, CH_2O $_{thf}$), 6.08 (d, $^3J_{H\text{-}H}$ = 7.8 Hz, 4H, H^5), 6.42 (d, $^3J_{H\text{-}H}$ = 7.7 Hz, 4H, H^3), 7.21 ppm (t, $^3J_{H\text{-}H}$ = 7.9 Hz, 4H, H^4). ^{13}C NMR (C_6D_6, 150.90 MHz, 298 K): δ = 1.89 ($(CH_3)_3Si$), 14.35 (CH_3 $_{n\text{-hexane}}$), 23.06 (CH_2CH_3 $_{n\text{-hexane}}$), 25.54 (CH_2CH_2O $_{thf}$), 31.97 ($CH_2CH_2CH_3$ $_{n\text{-hexane}}$), 68.10 (CH_2O $_{thf}$), 95.29 (C^3), 101.95 (C^5), 139.70 (C^4), 167.12 (C^2), 169.67 ppm (C^6).

3. Results and Discussion

3.1. H_5A and H_3L

The synthesis of H_5A (Figure 1) [38,40–42] was first described in 1947 by Bernstein et al. [38]. These authors isolated the crude monohydrochloride (H_5A·HCl) in 60% yield by the high-temperature solvent-less condensation of dap and dap·HCl in equimolar amounts (Scheme 1a), and converted it into the free base by aqueous alkali (Scheme 1b). Unfortunately, the overall yield was not quoted in the original paper. The procedure was replicated in ref. [41] and recently modified in the challenging purification step [40] with declared yields of 41% and 15%, respectively. We now provide a detailed reaction and work-up procedure that affords crystalline H_5A in ca. 46% overall yield (see Materials and Methods). Heating of the mixed reactants to 190 °C under N_2 results in a lively evolution of NH_3 and the initially liquid reaction mixture turns into a black hard solid over 2.5–3 days (H_5A·HCl is described as an infusible solid in ref. [38]). A fraction of such solid, presumably polymeric in nature, was found insoluble in water as well as in organic solvents such as DMSO, *i*-PrOH, EtOH, and benzene. According to ^{1}H NMR spectroscopy, the DMSO soluble fraction contains H_5A·HCl and dap·HCl in an approximately 3:1 molar ratio. The work-up involves prolonged extraction of H_5A·HCl in hot EtOH and liberation of the free base by treatment with aqueous alkali, which affords analytically and spectroscopically pure H_5A.

According to an X-ray powder diffraction study (Figure S1), the sample is mainly constituted by the crystal phase (α-H_5A) reported by Schrage et al. (unit cell parameters at 100 K: a = 9.7478(3), b = 7.6884(2), c = 13.4222(4) Å, β = 108.3800(10)°, V = 954.61(5) Å^3, Z = 4, $P2_1/n$) [40]. We also obtained X-ray quality crystals of α-H_5A following their procedure, namely evaporation of a chloroform solution. However, a set of extra peaks in the powder diffractogram, unaccounted for by α-H_5A, indicates the occurrence of a second polymorph. We were able to isolate this second crystal phase (β-H_5A) and to determine its structure by single-crystal methods (Table S1). β-H_5A belongs to monoclinic space group *Cc* and the asymmetric unit consists of two distinct molecules (mol1: N1-N5; mol2: N6-N10), both exhibiting a *cis-cis* conformation (Figure 2) [10]. Two complementary N-H···N hydrogen bonds are formed between the primary amino nitrogens N1 and N10, and the pyridine nitrogens N7 and N4. The remaining nitrogen atoms N2, N5, N6, and N9 are engaged in a similar pattern of hydrogen bonds with asymmetric units translated by ±1 along the y axis, thereby linking H_5A molecules into zig-zag chains parallel to y. Neighboring chains interact along z via longer H-contacts between primary amino nitrogen's (H···N ≅ 2.5 Å), while crystal cohesion along x is ensured by Van der Waals forces. It should be noted that secondary amino nitrogens (N3 and N8) are not involved in hydrogen bonds. To reduce repulsive interactions between β-hydrogens, the two pyridine rings are not coplanar, but form dihedral angles of 28.4° (mol1) and 30.1° (mol2).

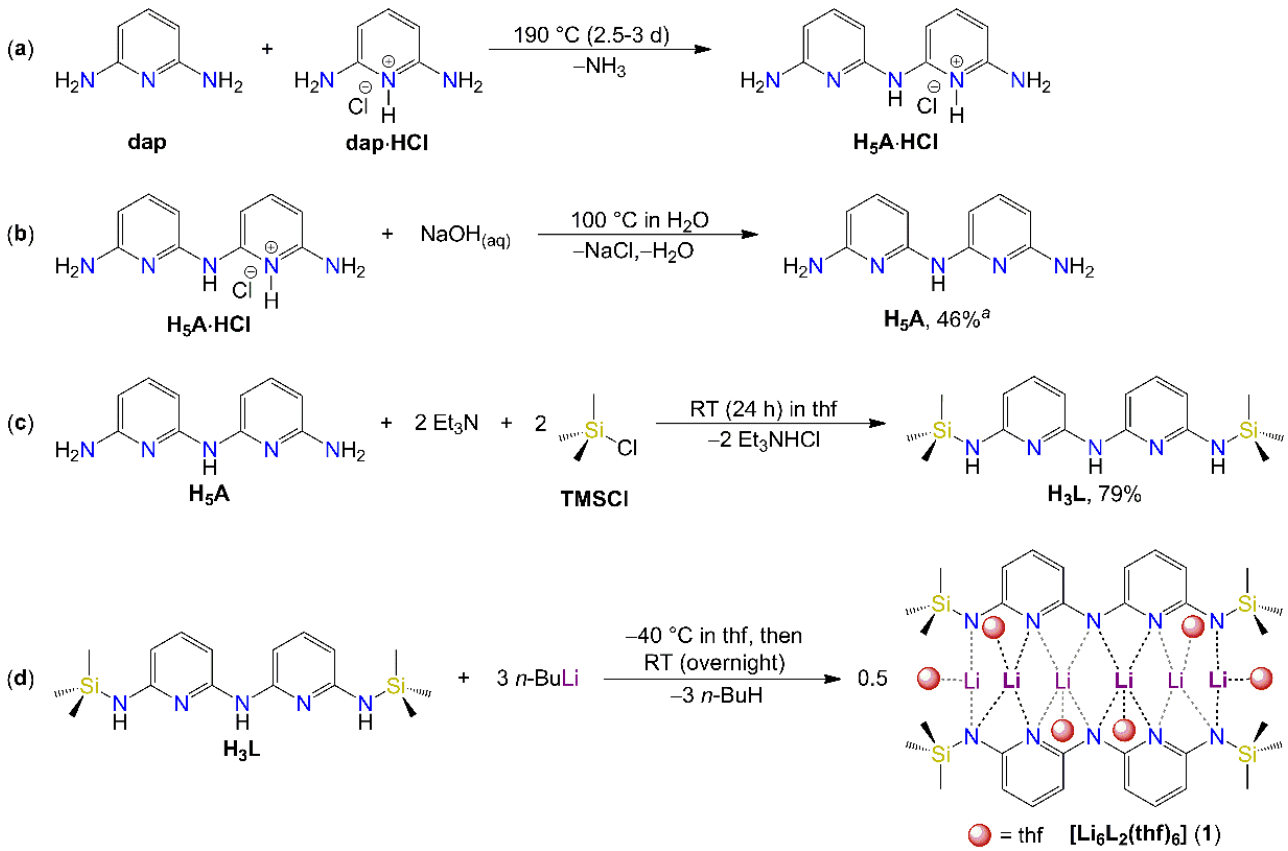

Scheme 1. Synthetic route to $H_5A{\cdot}HCl$, H_5A, H_3L, and **1** (RT = room temperature). (**a**) Condensation reaction between dap and dap·HCl; (**b**) neutralization to liberate the free amine H_5A; (**c**) double trimethylsilylation of H_5A; (**d**) lithiation of H_3L. [a]Overall yield of steps **a** and **b** obtained in this work.

In the polymorph described by Schrage et al. (α-H_5A) [40], the H_5A molecule also exhibits a *cis-cis* conformation. However, the dihedral angle between the two pyridine rings is significantly larger (47.3°) and no complementary hydrogen bonds are formed within molecular pairs; by consequence, the crystal packing is totally different and is dominated by a single hydrogen bond between a primary amino group and a pyridine nitrogen (H···N = 2.15 Å); secondary amino nitrogens are also not engaged in hydrogen bonding. It has to be noted that the monohydrochloride salt of H_5A, isolated by Schrage et al. as $H_5A{\cdot}HCl{\cdot}0.5EtOH{\cdot}0.5H_2O$ [40], exhibits a *trans-trans* conformation [10] with an intramolecular H-bond between the two pyridine nitrogen atoms, one of which is protonated.

Double trimethylsilylation of H_5A to give symmetric H_3L was accomplished by reaction with a slightly over-stoichiometric amount of TMSCl in thf/Et_3N at room temperature (Scheme 1c) [7,43]. In these conditions, silylation occurs exclusively on the primary amino groups, as clearly shown by NMR spectroscopy (Figures S7–S9), and over-silylation was never observed for up to 3 equivs. of TMSCl. The product, although not crystalline, is sufficiently pure for the subsequent lithiation step.

3.2. $[Li_6L_2(thf)_6]{\cdot}C_6H_{14}$ (**1**$\cdot C_6H_{14}$)

Lithiation of H_3L was carried out using a slightly over-stoichiometric amount of *n*-BuLi in thf (Scheme 1d). The crude product so obtained is fairly soluble in hydrocarbons. Its ^{1}H NMR spectrum in benzene-d_6 contains a single $(CH_3)_3Si$ resonance and three aromatic signals of equal integrated intensity (one triplet and two doublets), as expected for a twofold symmetric L^{3-} moiety (Figures S10–S12). No evidence for residual N-H groups emerged from the spectrum. Signals from thf molecules were instead clearly observed at

3.27 and 1.22 ppm, that is, at significantly different chemical shifts from uncoordinated thf in benzene-d_6 (3.57 and 1.40 ppm) [26]. Their integrated intensities are indicative of three thf molecules per L^{3-} ligand.

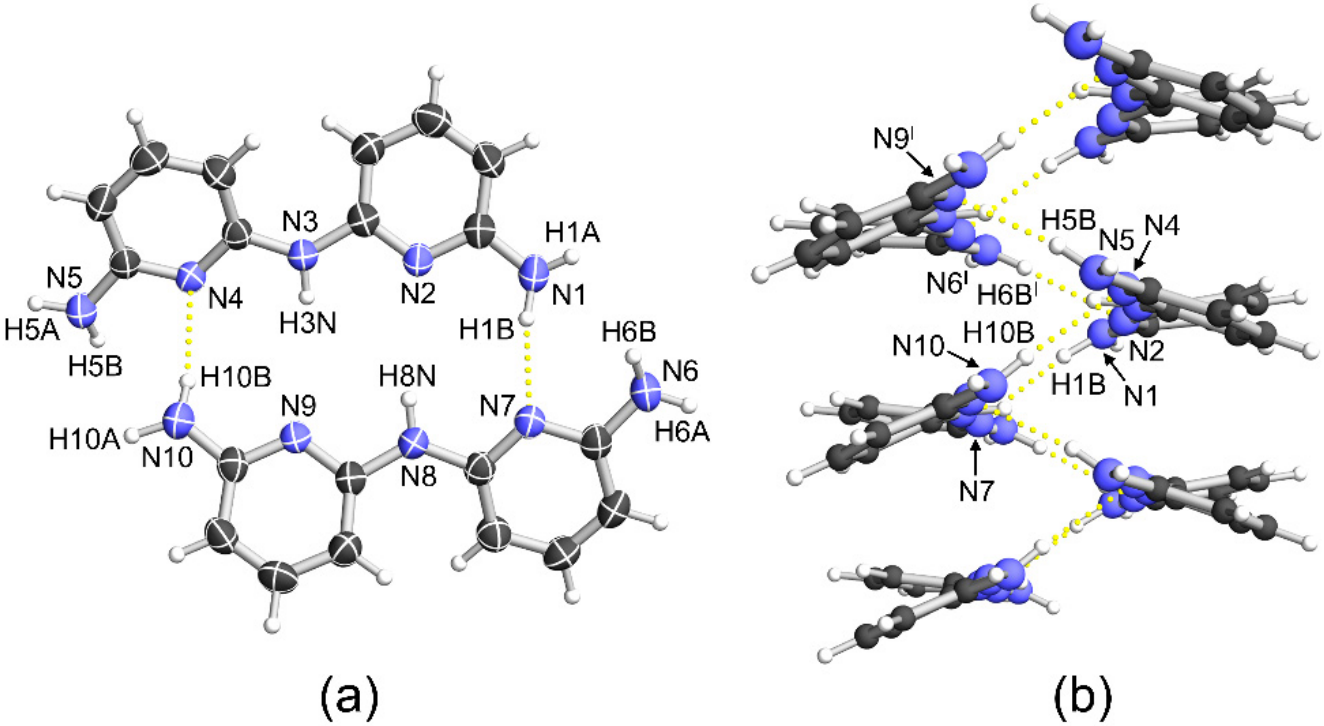

Figure 2. Crystal structure of β-H_5A, viewed approximately perpendicular (**a**) and parallel (**b**) to the average plane through the asymmetric unit. Color code: C (dark gray), N (blue), and H (white). Thermal ellipsoids in (**a**) are at 60% probability level, while H atoms in (**a**) and all atoms in (**b**) are drawn as spheres of arbitrary radius. Yellow dotted lines indicate hydrogen bonds. Selected interatomic distances and angles: H1B···N7 = 2.24(4) Å, N1-H1B···N7 = 168(2)°; H10B···N4 = 2.25(4) Å, N10-H10B···N4 = 170(3)°; H5B···$N9^I$ = 2.20(4) Å, N5-H5B···$N9^I$ = 166(3)°; $H6B^I$···N2 = 2.29(4) Å, $N6^I$-$H6B^I$···N2 = 168(3)°. Symmetry code: I = x, y + 1, z.

Recrystallization from *n*-hexane/thf 10:1 (v/v) at −20 °C gave crystals belonging to orthorhombic space group *Pbcn* (Table S1). Their unit cell contains four hexalithium complexes (**1**) and four interstitial *n*-hexane molecules. Complex **1** (Figure 3 and Table 1) develops around a twofold axis which passes through N3 and N6 and is parallel to the y crystal axis. Consequently, it has crystallographic C_2 symmetry. The two L^{3-} ligands are twisted from each other by approximately 60° (vide infra) and convey to the molecule a helical structure. They adopt a *cis-cis* conformation and feature three different types of nitrogen donors, all of which are metal-coordinated: amido-type nitrogens bound to two pyridine rings (N_{am} = N3, N6), amido-type nitrogens connected to a pyridine ring and to the $(CH_3)_3Si$ group (N_{TMS} = N1, N4), and pyridine-type nitrogens (N_{py} = N2, N5). All nitrogen atoms, except for N_{TMS}-type donor N4, act as bridges between two metal ions. Each Li^+ ion is coordinated by the O atom of a thf molecule and by two (Li1), three (Li2), or four (Li3) nitrogen donors from the L^{3-} ligands. Li1 resides in a trigonal planar $O(N_{TMS})_2$ environment, Li2 has a very distorted tetrahedral $O(N_{TMS})(N_{py})_2$ environment, and Li3 has a very distorted rectangular pyramidal $O(N_{am})_2(N_{py})_2$ coordination, with a long Li-N_{py} bond (Li3-N2 = 2.407(3) Å). Li-Li distances range from 2.578(4) Å (Li1-Li2) to 3.359(4) Å (Li1-Li3). The central core, as defined by Li3 and $Li3^I$, bears direct resemblance to the structure of $[Li_2(dpa)_2(2\text{-MeTHF})_2]$ [21]; evidently, functionalization of Hdpa with two additional (trimethylsilyl)amino groups allows the structure to expand incorporating four more Li^+ ions.

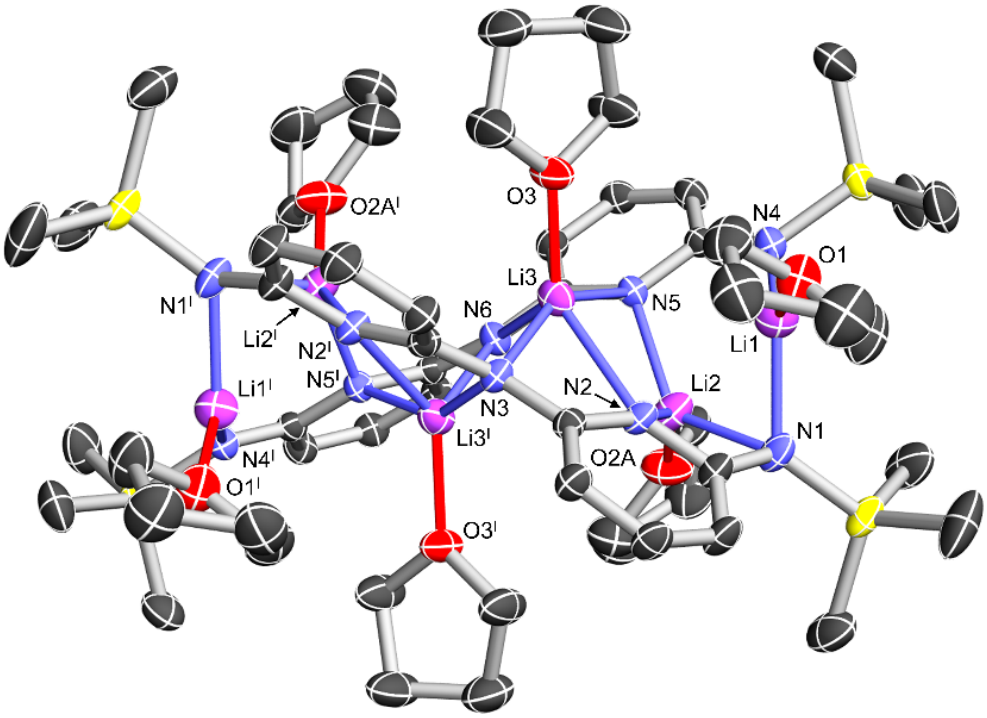

Figure 3. Molecular structure of **1**, viewed approximately along the twofold axis passing through N3 and N6. Color code: Li (purple), C (dark gray), N (blue), O (red), and Si (yellow). Thermal ellipsoids are at 60% probability level. Hydrogen atoms and the minority component of the disordered thf molecule bound to Li2 are omitted for clarity. Atoms with symmetry code "I" are obtained by rotation around the twofold axis.

Table 1. Most significant interatomic distances (Å) in **1**·C_6H_{14} and **2**.

	1·C_6H_{14} [1]			**2 (mol1)** [2]			**2 (mol2)** [3]	
Li1	Li2	2.578(4)	Li1	Li2	2.361(6)	Li7	Li8	2.353(6)
	Li3	3.359(4)		Li3	3.216(6)		Li9	3.103(6)
	O1	1.951(3)		O1	1.913(4)		O5	1.901(4)
	N1	2.032(3)		N1	2.041(5)		N11	2.055(4)
	N4	1.983(3)		N6	2.020(4)		N16	2.037(4)
Li2	Li3	2.729(4)	Li2	Li3	2.915(6)	Li8	Li9	3.002(6)
	O2A	1.896(10)		O2	1.920(4)		O6A	1.908(13)
	O2B	1.981(12)		N1	2.042(4)		O6B	1.95(3)
	N1	2.112(3)		N6	2.097(4)		N11	2.022(4)
	N2	2.150(3)		N7	2.335(5)		N16	2.104(4)
	N5	2.065(3)					N17	2.453(5)
Li3	Li3^{I}	2.595(5)	Li3	Li4	2.441(5)	Li9	Li10	2.424(5)
	O3	1.967(3)		N2	1.965(4)		N12	1.985(4)
	N2	2.407(3)		N3	2.107(4)		N13	2.110(4)
	N3	2.015(3)		N7	1.992(4)		N17	1.985(4)
	N5	2.084(3)		N8	2.101(4)		N18	2.106(4)
	N6	2.179(3)						
			Li4	Li5	2.970(6)	Li10	Li11	3.077(6)
				Li6	3.099(6)		Li12	2.975(6)
				N3	2.086(4)		N13	2.092(4)
				N4	1.976(4)		N14	1.977(4)
				N8	2.107(4)		N18	2.094(4)
				N9	1.970(4)		N19	1.975(4)

Table 1. *Cont.*

1·C_6H_{14} [1]		**2 (mol1)** [2]		**2 (mol2)** [3]
	Li5	Li6 2.371(6) O3 1.906(4) N5 2.033(4) N9 2.365(5) N10 2.077(4)	Li11	Li12 2.370(6) O7 1.917(4) N15 2.033(4) N20 2.074(5)
	Li6	O4 1.913(4) N5 2.066(5) N10 2.029(5)	Li12	O8A 1.924(12) O8B 1.93(2) N14 2.375(5) N15 2.093(4) N20 2.024(4)

[1] Next-longest Li-N distance: Li1-N2, 2.624(3) Å; atoms Li3 and Li3^{I} are related by rotation around the twofold axis passing through N3 and N6. [2] Next-longest Li-N distances: Li1-N2, 2.682(5) Å; Li6-N4, 2.545(5) Å. [3] Next-longest Li-N distances: Li7-N12 2.558(5) Å; Li11-N19 2.484(5) Å.

A ^{1}H, ^{13}C, ^{15}N, and ^{7}Li NMR characterization was carried out on solutions prepared by dissolving crystalline **1**·C_6H_{14} in benzene-d_6. Apart from the additional *n*-hexane peaks, the room-temperature ^{1}H spectrum (Figures S13–S15) is virtually identical to that recorded on the crude product (Figures S10–S12). In agreement with the number of distinct proton resonances, six L^{3-} signals are observed in the ^{13}C spectrum (Figure S16), confirming that all pyridyl and trimethylsilyl groups are equivalent on NMR time scale. This result is consistent with the solid-state structure provided that the effective molecular symmetry increases from C_2 to D_2. Additional spectra pointed to only marginal temperature dependence between 283 and 310 K (Figures S17–S20, S26–S28).

Complete assignment of all ^{1}H and ^{13}C resonances was accomplished using a combination of ^{1}H-^{1}H COSY, ^{1}H-^{13}C HSQC, ^{1}H-^{13}C HMBC, and ^{1}H-^{1}H ROESY experiments carried out at 283 K (Figures S21–S24 and Table S2). In particular, the cross-peak between $(CH_3)_3Si$ and H^5 signals at 0.52 and 6.08 ppm, respectively, in the ROESY spectrum permits an unambiguous assignment of the two β-hydrogens of the pyridine rings (Figure S24). Moreover, the same spectrum shows an evident cross-peak between the $(CH_3)_3Si$ signal and the CH_2O protons of thf at 3.36 ppm, as well as a lower one with the CH_2CH_2O protons at 1.25 ppm. This indicates that L^{3-} and thf are close in space and part of the same molecule. Additionally, in the ^{1}H-^{15}N HMBC spectrum recorded at the same temperature (Figure S25) the $(CH_3)_3Si$ hydrogens give a clear cross-peak with an N atom resonating at 118.3 ppm, and thus attributed to N_{TMS}. Both β-hydrogens afford the expected cross-peak with N_{py} at 225.4 ppm, while the signal from N_{am} escaped detection.

A careful analysis of the ^{1}H NMR spectrum revealed a set of very weak signals with identical integrated intensity (1H), namely three triplets in the γ-H region, six doublets in the β-H region, and one singlet at 3.84 ppm (at 283 K). In addition, three weak singlets (~9H) are detected in the $(CH_3)_3Si$ region (Table S3). We assign this signal set, which exhibited a strongly batch-dependent intensity, to an impurity containing one HN_{TMS} group and displaying no internal symmetry, e.g., $[Li_5(HL)L(thf)_x]$ (**3**). This structure would in fact give rise to four γ-H triplets, eight β-H doublets, one NH singlet, and four $(CH_3)_3Si$ signals, some of which may well be hidden under the dominant peaks.

The ^{7}Li NMR spectrum, recorded at 283 K, is dominated by a singlet at 2.03 ppm (Figure S29) and features a much weaker signal at 1.29 ppm. This result is surprising considering the presence of inequivalent lithium environments in the solid state, but is not unprecedented [44,45]. Examination of different synthetic batches showed that the relative contributions of minority signals to the ^{7}Li and ^{1}H spectra are correlated and consistent with the presence of up to a few mol% of **3**. Both the dominant and the minority ^{7}Li peaks become narrower when heating the sample to 310 K (Figure S29). This behavior agrees with the occurrence of fast chemical exchange among the unique Li^+ ions in the structure, and a slowing down of the process with decreasing temperature.

A *MW* estimation was obtained from diffusion ordered spectroscopy (^{1}H DOSY) (Figure S30) [46]. The normalized diffusion coefficient $D_{x,norm}$ = 5.21 × 10^{-10} m^2 s^{-1} determined for **1** in benzene-d_6 at 298 K yields *MW* = 950 and 822 using the ECC_{merge} and ECC_{DSE} parameters, respectively, proposed by Bachmann et al. [28]. These values lie outside the *MW* range explored by those authors and must be taken with care [47]. However, comparison with *MW*s calculated for **1** (1159), **2** (1015), and thf-free [Li_6L_2] (727) clearly indicates that the solution structure of **1** still contains pairs of L^{3-} ligands. Interestingly, the normalized diffusion coefficient of thf determined from its CH_2O signal (1.04 × 10^{-9} m^2 s^{-1}) is higher than that of **1** but lower than for free thf in benzene-d_6 (2.31 × 10^{-9} m^2 s^{-1}) [28]. This proves that bound thf is fast exchanging with some free thf. The percentages of bound and free thf can be estimated considering that the measured diffusion coefficient is a weighted average of free and bound thf forms [48]. If we assign to bound thf the same diffusion coefficient as **1**, we can estimate that the fraction of free thf is about 30%. Hence, our combined NMR investigations converge in indicating that the solid-state structure of **1** is retained in benzene-d_6 solution, although with a higher (D_2) symmetry on NMR time scale and a significant fraction of dissociated thf ligands.

*3.3. [$Li_6L_2(thf)_4$] (**2**)*

In an early attempt to recrystallize crude **1** by evaporation of an *n*-hexane solution, we occasionally isolated crystals of the same hexalithium salt, but containing only four coordinated thf molecules, [$Li_6L_2(thf)_4$] (**2**). The different extent of solvation leads to important structural differences. Crystals belong to triclinic space group $P\bar{1}$ (Table S1) and the asymmetric unit contains two inequivalent molecules (mol1: Li1-Li6; mol2: Li7-Li12), which are oriented almost parallel inside the unit cell (Figures 4 and 5, and Table 1). All nitrogen atoms, except for N_{py}-type donors N2 and N4 in mol1, and N12 and N19 in mol2 act as bridges between two metal ions. As compared with **1**, the thf ligands on the inner Li^+ ions (Li3, Li4, Li9, and Li10) are missing in both molecules; these ions approach a rectangular planar $(N_{am})_2(N_{py})_2$ coordination (sum of N-Li-N angles = 364.7–365.6°) and are significantly closer to each other than in **1** (2.42–2.44 vs. 2.60 Å). The remaining four outer Li^+ ions per molecule are arranged in two pairs. The metal ions within each pair lie on opposite sides of the average molecular plane, which can be taken to coincide with the central Li_2N_2 moiety. They are much closer to each other (2.35–2.37 Å) than to the neighboring inner ions (2.92–3.22 Å) and have distinctly different coordination geometries. Li1, Li6, Li7, and Li11 have the same trigonal planar $O(N_{TMS})_2$ environment as Li1 in **1**. By contrast, Li2, Li5, Li8, and Li12 are four-coordinated, but with an $O(N_{TMS})_2(N_{py})$ environment rather than the $O(N_{TMS})(N_{py})_2$ donor set of Li2 in **1**. In each molecule, these outer metal pairs and the bridging N_{TMS} donors define two terminal $Li_2(N_{TMS})_2$ quadrangles, which are rotated away from each other by approximately 90° as a consequence of the helical arrangement of the ligands. A subtle structural difference between the two crystallographically-independent molecules in **2** is the position of the two three-coordinated Li^+ ions. Li1 and Li6 in mol1 lie on opposite sides of the average molecular plane (as in **1**), whereas Li7 and Li11 in mol2 lie on the same side. The absence of thf coordination on the inner metal sites leads to a different extent of twisting between the two *cis-cis* L^{3-} ligands. This is shown by the dihedral angle between C-N_{am}-C planes, which is 61.2° in **1**, 52.6° in mol1 of **2**, and 52.2° in mol2 of **2**. Along with a reduced ligand twisting, **2** entails a smaller dihedral angle between neighboring pyridine rings within the same ligand (50.1° in **1**, 38.2–40.1° in **2**). Thus, **2** features a more planar core structure and a smaller helical pitch than **1**.

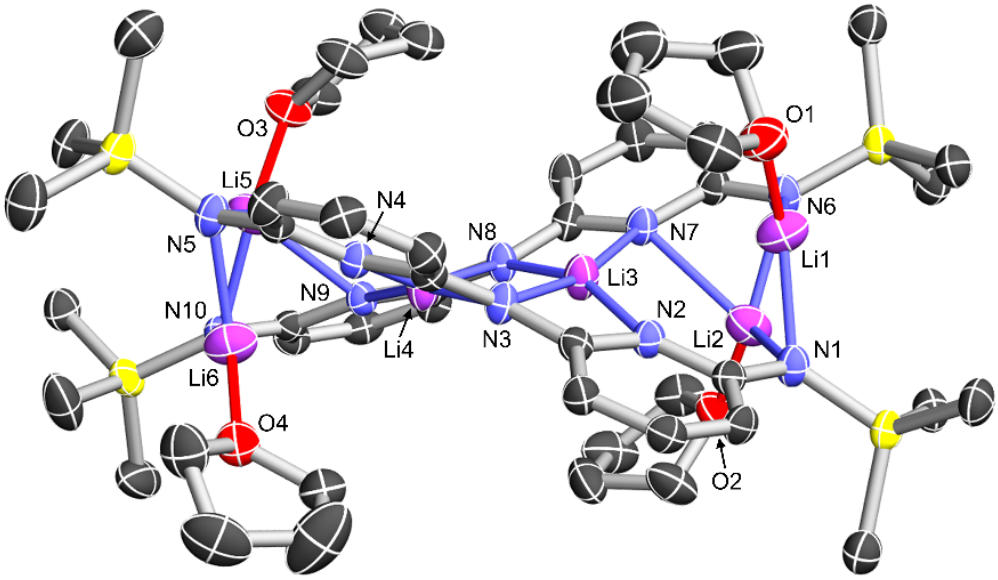

Figure 4. Molecular structure of mol1 in **2**, viewed approximately along the line joining N3 and N8. Same color code as in Figure 3. Thermal ellipsoids are at 60% probability level and hydrogen atoms are omitted for clarity.

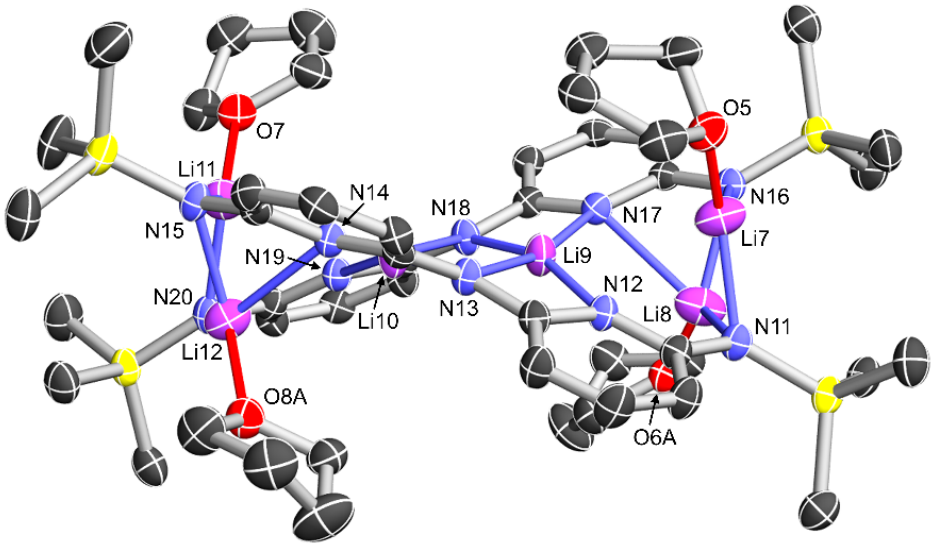

Figure 5. Molecular structure of mol2 in **2**, viewed approximately along the line joining N13 and N18. Same color code as in Figure 3. Thermal ellipsoids are at 60% probability level. Hydrogen atoms and the minority components of the disordered thf molecules bound to Li8 and Li12 are omitted for clarity.

4. Conclusions

The synthetic path to compound H_5A, featuring alternating α-pyridyl and amino groups, was consolidated and shown to afford a mixture of two polymorphs. H_5A undergoes trimethylsilylation on its primary amino groups to yield H_3L, which contains three secondary NH functions. Its reaction with *n*-BuLi in thf affords compound $[Li_6L_2(thf)_6]$ (**1**), which crystallizes from *n*-hexane/thf as **1**·C_6H_{14}. A related compound (**2**) with only four thf ligands per molecule was also isolated. These crystalline salts comprise a pair of fully deprotonated, twisted L^{3-} ligands adopting a *cis-cis* conformation and using all their five N donors for coordination to the six Li^+ ions. According to NMR studies, this dimeric structure is largely maintained in benzene-d_6 solution.

To the best of our knowledge, the herein reported hexalithium compounds are the longest-chain lithium oligo-α-pyridylamides structurally authenticated so far. They are currently under testing in our laboratory as intermediates for the synthesis of new high-nuclearity EMACs following Cotton's *trans-metalation* method [15]. In particular, the L^{3-} ligands in **1** and **2** contain five N donors and three negative charges, as opposed—for instance—to the five N donors and two negative charges of N^2,N^6-di(pyridin-2-yl)pyridine-2,6-diamido ($tpda^{2-}$) ligands [11,16–18]. This might expand the variety of accessible metal ion combinations and oxidation states in EMAC structures.

Supplementary Materials: The following supporting information can be downloaded at: https://www.mdpi.com/article/10.3390/chemistry4020037/s1, Figure S1: X-ray powder diffractogram of H_5A at room temperature; Figure S2: ^{1}H NMR spectrum of dap·HCl in $(CD_3)_2SO$ at 298 K; Figures S3 and S4: ^{1}H NMR spectrum of dap·HCl in $(CD_3)_2SO$ at 298 K (expanded regions); Figure S5: ^{1}H NMR spectrum of H_5A in $(CD_3)_2SO$ at 298 K; Figure S6: ^{1}H NMR spectrum of H_5A in $(CD_3)_2SO$ at 298 K (expanded region); Figure S7: ^{1}H NMR spectrum of H_3L in C_6D_6 at 298 K; Figure S8: ^{1}H NMR spectrum of H_3L in C_6D_6 at 298 K (expanded region); Figure S9: ^{13}C NMR spectrum of H_3L in C_6D_6 at 298 K; Figure S10: ^{1}H NMR spectrum of crude **1** in C_6D_6 at 298 K; Figures S11 and S12: ^{1}H NMR spectrum of crude **1** in C_6D_6 at 298 K (expanded regions); Figure S13: ^{1}H NMR spectrum of **1**·C_6H_{14} in C_6D_6 at 298 K; Figures S14 and S15: ^{1}H NMR spectrum of **1**·C_6H_{14} in C_6D_6 at 298 K (expanded regions); Figure S16: ^{13}C NMR spectrum of **1**·C_6H_{14} in C_6D_6 at 298 K; Figure S17: ^{1}H NMR spectrum of **1**·C_6H_{14} in C_6D_6 at 283 K; Figures S18 and S19: ^{1}H NMR spectrum of **1**·C_6H_{14} in C_6D_6 at 283 K (expanded regions); Figure S20: ^{13}C NMR spectrum of **1**·C_6H_{14} in C_6D_6 at 283 K; Figure S21: ^{1}H-^{1}H COSY spectrum of **1**·C_6H_{14} in C_6D_6 at 283 K; Figure S22: ^{1}H-^{13}C HSQCed spectrum of **1**·C_6H_{14} in C_6D_6 at 283 K; Figure S23: ^{1}H-^{13}C HMBC spectrum of **1**·C_6H_{14} in C_6D_6 at 283 K; Figure S24: ^{1}H-^{1}H ROESY spectrum of **1**·C_6H_{14} in C_6D_6 at 283 K; Figure S25: ^{1}H-^{15}N HMBC spectrum of **1**·C_6H_{14} in C_6D_6 at 283 K; Figure S26: ^{1}H NMR spectrum of **1**·C_6H_{14} in C_6D_6 at 310 K; Figures S27 and S28: ^{1}H NMR spectrum of **1**·C_6H_{14} in C_6D_6 at 310 K (expanded regions); Figure S29: ^{7}Li NMR spectrum of **1**·C_6H_{14} in C_6D_6 at three different temperatures; Figure S30: ^{1}H DOSY spectrum of **1**·C_6H_{14} in C_6D_6 at 298 K; Table S1: Crystal data and refinement parameters for β-H_5A, **1**·C_6H_{14}, and **2**; Table S2: Assignment of ^{1}H and ^{13}C NMR signals for **1**·C_6H_{14} in C_6D_6 at 283 K; Table S3: Impurity NMR signals for **1**·C_6H_{14} in C_6D_6 at 283 K.

Author Contributions: Conceptualization, A.C.; Methodology, A.M. and A.C.; Validation, A.M. and A.C.; Formal Analysis, A.M. and A.C.; Investigation, A.R., A.M., A.N. and A.C.; Resources, A.M. and A.C.; Data Curation, A.C.; Writing—Original Draft Preparation, A.C.; Writing—Review & Editing, A.R., A.M., A.N. and A.C.; Visualization, A.R., A.M., A.N. and A.C.; Supervision, A.C. All authors have read and agreed to the published version of the manuscript.

Funding: This research received no external funding.

Data Availability Statement: The data presented in this study are available in Supplementary Material.

Acknowledgments: We are grateful to Gary L. Guillet (Georgia Southern University, Savannah, GA, United States) for stimulating discussion and to Massimo Tonelli (Centro Interdipartimentale Grandi Strumenti, University of Modena and Reggio Emilia) for assistance in collecting X-ray powder diffraction data.

Conflicts of Interest: The authors declare no conflict of interest.

References

1. Chlupatý, T.; Růžička, A. Hybrid amidinates and guanidinates of main group metals. *Coord. Chem. Rev.* **2016**, *314*, 103–113. [CrossRef]
2. Zechovský, J.; Mrózek, O.; Samsonov, M.; Jambor, R.; Růžička, A.; Dostál, L. Coordination capabilities of bis-(2-pyridyl)amides in the field of divalent germanium, tin and lead compounds. *Dalton Trans.* **2021**, *50*, 6321–6332. [CrossRef]
3. Kempe, R. The Strained η^2-$N_{Amido}-N_{Pyridine}$ Coordination of Aminopyridinato Ligands. *Eur. J. Inorg. Chem.* **2003**, *2003*, 791–803. [CrossRef]
4. Berry, J.F.; Cotton, F.A.; Daniels, L.M.; Murillo, C.A.; Wang, X. Oxidation of $Ni_3(dpa)_4Cl_2$ and $Cu_3(dpa)_4Cl_2$: Nickel−Nickel Bonding Interaction, but No Copper−Copper Bonds. *Inorg. Chem.* **2003**, *42*, 2418–2427. [CrossRef]

5. Chen, P.-J.; Sigrist, M.; Horng, E.-C.; Lin, G.-M.; Lee, G.-H.; Chen, C.-h.; Peng, S.-M. A ligand design with a modified naphthyridylamide for achieving the longest EMACs: The 1st single-molecule conductance of an undeca-nickel metal string. *Chem. Commun.* **2017**, *53*, 4673–4676. [CrossRef] [PubMed]
6. Aoki, K.; Otsubo, K.; Yoshida, Y.; Kimura, Y.; Sugimoto, K.; Kitagawa, H. Synthesis and Magnetic Properties of a Dimerized Trinuclear Ni String Complex, $[Ni_6Cl_2(dpa)_8](I_5)_2 \cdot 0.25I_2$ (dpa^- = 2,2′-Dipyridylamide Anion). *Inorg. Chem.* **2021**, *60*, 16029–16034. [CrossRef]
7. Guillet, G.L.; Arpin, K.Y.; Boltin, A.M.; Gordon, J.B.; Rave, J.A.; Hillesheim, P.C. Synthesis and Characterization of a Linear Triiron(II) Extended Metal Atom Chain Complex with Fe–Fe Bonds. *Inorg. Chem.* **2020**, *59*, 11238–11243. [CrossRef]
8. Cotton, F.A.; Murillo, C.A.; Wang, X. Trinuclear complexes of copper, cobalt and iron with *N*,*N*′-di(2-pyridyl) formamidinate ligands, $[M_3(DPyF)_4][PF_6]_2$. *Inorg. Chem. Commun.* **1998**, *1*, 281–283. [CrossRef]
9. Srinivasan, A.; Musgrave, R.A.; Rouzières, M.; Clérac, R.; McGrady, J.E.; Hillard, E.A. A linear metal–metal bonded tri-iron single-molecule magnet. *Chem. Commun.* **2021**, *57*, 13357–13360. [CrossRef]
10. Brogden, D.W.; Berry, J.F. Coordination Chemistry of 2,2′-Dipyridylamine: The Gift That Keeps on Giving. *Comments Inorg. Chem.* **2016**, *36*, 17–37. [CrossRef]
11. Hua, S.-A.; Cheng, M.-C.; Chen, C.-h.; Peng, S.-M. From Homonuclear Metal String Complexes to Heteronuclear Metal String Complexes. *Eur. J. Inorg. Chem.* **2015**, *2015*, 2510–2523. [CrossRef]
12. Berry, J.F.; Cotton, F.A.; Murillo, C.A.; Chan, Z.-K.; Yeh, C.-W.; Chen, J.-D. Linear Trichromium, Tricobalt, Trinickel, and Tricopper Complexes of 2,2′-Dipyridylamide. *Inorg. Synth.* **2014**, *36*, 103–110. [CrossRef]
13. Hurley, T.J.; Robinson, M.A. Nickel(II)-2,2′-dipyridylamine system. I. Synthesis and stereochemistry of the complexes. *Inorg. Chem.* **1968**, *7*, 33–38. [CrossRef]
14. Yang, E.-C.; Cheng, M.-C.; Tsai, M.-S.; Peng, S.-M. Structure of a linear unsymmetrical trinuclear cobalt(II) complex with a localized Co^{II}–Co^{II} bond: Dichlorotetrakis[μ_3-bis(2-pyridyl)amido]tricobalt(II). *J. Chem. Soc. Chem. Commun.* **1994**, 2377–2378. [CrossRef]
15. Cotton, F.A.; Daniels, L.M.; Murillo, C.A.; Pascual, I. Compounds with linear, bonded trichromium chains. *J. Am. Chem. Soc.* **1997**, *119*, 10223–10224. [CrossRef]
16. Nicolini, A.; Galavotti, R.; Barra, A.-L.; Borsari, M.; Caleffi, M.; Luo, G.; Novitchi, G.; Park, K.; Ranieri, A.; Rigamonti, L.; et al. Filling the Gap in Extended Metal Atom Chains: Ferromagnetic Interactions in a Tetrairon(II) String Supported by Oligo-α-pyridylamido Ligands. *Inorg. Chem.* **2018**, *57*, 5438–5448. [CrossRef]
17. Nicolini, A.; Affronte, M.; SantaLucia, D.J.; Borsari, M.; Cahier, B.; Caleffi, M.; Ranieri, A.; Berry, J.F.; Cornia, A. Tetrairon(II) extended metal atom chains as single-molecule magnets. *Dalton Trans.* **2021**, *50*, 7571–7589. [CrossRef]
18. Chipman, J.A.; Berry, J.F. Paramagnetic Metal–Metal Bonded Heterometallic Complexes. *Chem. Rev.* **2020**, *120*, 2409–2447. [CrossRef]
19. Glatz, G.; Kempe, R. Crystal structure of bis-μ_3(*N*,*N*′-bis-(trimethylsilyl)-pyridine-2-amine-6-amido)-μ_4(*N*,*N*′-bis-(trimethylsilyl)-pyridine-2,6-diamido)-di-tetrahydrofuran-tetralithium, $[(C_{11}H_{21}N_3Si_2)(C_{11}H_{22}N_3Si_2)_2(C_4H_8O)_2Li_4]$. *Z. Kristallogr. New Cryst. Struct.* **2008**, *223*, 307–308. [CrossRef]
20. Skvortsov, G.G.; Fukin, G.K.; Ketkov, S.Y.; Cherkasov, A.V.; Lyssenko, K.A.; Trifonov, A.A. Benzonitrile Insertion into Silylarylamides—*ansa*-Bis(benzamidinate) Ligand Systems with Rigid *o*- and *m*-Phenylene Linkers in the Synthesis of Lithium and Rare Earth Complexes. *Eur. J. Inorg. Chem.* **2013**, *2013*, 4173–4183. [CrossRef]
21. Fairley, M.; Bole, L.J.; Mulks, F.F.; Main, L.; Kennedy, A.R.; O'Hara, C.T.; García-Alvarez, J.; Hevia, E. Ultrafast amidation of esters using lithium amides under aerobic ambient temperature conditions in sustainable solvents. *Chem. Sci.* **2020**, *11*, 6500–6509. [CrossRef] [PubMed]
22. Armarego, W.L.F.; Chai, C.L.L. *Purification of Laboratory Chemicals*, 5th ed.; Elsevier, Ed.; Butterworth-Heinemann: Burlington, VT, USA, 2003; ISBN 0-7506-7571-3.
23. den Hertog, H.J.; Wibaut, J.P. On the reactivity of bromine atoms in brominated pyridines. Preparation of some 2:6-disubstitution products of pyridine. *Recl. Trav. Chim. Pays-Bas* **1936**, *55*, 122–130. [CrossRef]
24. Love, B.E.; Jones, E.G. The Use of Salicylaldehyde Phenylhydrazone as an Indicator for the Titration of Organometallic Reagents. *J. Org. Chem.* **1999**, *64*, 3755–3756. [CrossRef] [PubMed]
25. Matuszak, C.A.; Matuszak, A.J. Readily available anhydrous ether solutions of hydrogen chloride. *J. Chem. Educ.* **1967**, *44*, 108. [CrossRef]
26. Fulmer, G.R.; Miller, A.J.M.; Sherden, N.H.; Gottlieb, H.E.; Nudelman, A.; Stoltz, B.M.; Bercaw, J.E.; Goldberg, K.I. NMR Chemical Shifts of Trace Impurities: Common Laboratory Solvents, Organics, and Gases in Deuterated Solvents Relevant to the Organometallic Chemist. *Organometallics* **2010**, *29*, 2176–2179. [CrossRef]
27. Wu, D.H.; Chen, A.D.; Johnson, C.S. An Improved Diffusion-Ordered Spectroscopy Experiment Incorporating Bipolar-Gradient Pulses. *J. Magn. Reson. Ser. A* **1995**, *115*, 260–264. [CrossRef]
28. Bachmann, S.; Neufeld, R.; Dzemski, M.; Stalke, D. New External Calibration Curves (ECCs) for the Estimation of Molecular Weights in Various Common NMR Solvents. *Chem. Eur. J.* **2016**, *22*, 8462–8465. [CrossRef]
29. Bachmann, S.; Gernert, B.; Stalke, D. Solution structures of alkali metal cyclopentadienides in THF estimated by ECC-DOSY NMR-spectroscopy (incl. software). *Chem. Commun.* **2016**, *52*, 12861–12864. [CrossRef]
30. *APEX2, SADABS, SAINT*; Bruker-AXS, Inc.: Madison, WI, USA, 2012.

31. Altomare, A.; Cascarano, G.; Giacovazzo, C.; Guagliardi, A.; Burla, M.C.; Polidori, G.; Camalli, M. SIR 92—A program for automatic solution of crystal structures by direct methods. *J. Appl. Crystallogr.* **1994**, *27*, 435. [CrossRef]
32. Sheldrick, G.M. Crystal structure refinement with SHELXL. *Acta Crystallogr. Sect. C Struct. Chem.* **2015**, *71*, 3–8. [CrossRef]
33. Farrugia, L.J. WinGX and ORTEP for Windows: An update. *J. Appl. Crystallogr.* **2012**, *45*, 849–854. [CrossRef]
34. Thorn, A.; Dittrich, B.; Sheldrick, G.M. Enhanced rigid-bond restraints. *Acta Crystallogr. Sect. A Found. Crystallogr.* **2012**, *68*, 448–451. [CrossRef]
35. *Persistence of Vision Raytracer (Version 3.7) [Computer software]*; Persistence of Vision Pty. Ltd.: Williamstown, Australia, 2013; Available online: http://www.povray.org/download/ (accessed on 24 May 2022).
36. Macrae, C.F.; Sovago, I.; Cottrell, S.J.; Galek, P.T.A.; McCabe, P.; Pidcock, E.; Platings, M.; Shields, G.P.; Stevens, J.S.; Towler, M.; et al. Mercury 4.0: From visualization to analysis, design and prediction. *J. Appl. Crystallogr.* **2020**, *53*, 226–235. [CrossRef] [PubMed]
37. Bernstein, J.; Stearns, B.; Dexter, M.; Lott, W.A.I. Derivatives of Aminopyridines. *J. Am. Chem. Soc.* **1947**, *69*, 1147–1150. [CrossRef]
38. Bernstein, J.; Stearns, B.; Shaw, E.; Lott, W.A., II. Derivatives of 2,6-Diaminopyridine. *J. Am. Chem. Soc.* **1947**, *69*, 1151–1158. [CrossRef]
39. Mibu, N.; Yokomizo, K.; Miyata, T.; Sumoto, K. *N*-Monocarbamoyl Derivatives of Symmetrical Diamines with Antiviral Activity. *Chem. Pharm. Bull.* **2007**, *55*, 1406–1411. [CrossRef]
40. Schrage, B.R.; Chanawanno, K.; Crandall, L.A.; Ziegler, C.J. The synthesis of a hexameric expanded hemiporphyrazine. *J. Porphyr. Phthalocyanines* **2020**, *24*, 129–134. [CrossRef]
41. Lemport, P.S.; Ostapchuk, P.N.; Bobrikova, A.A.; Petrovskii, P.V.; Kagramanov, N.D.; Bodrin, G.V.; Nifant'ev, E.E. Direct phosphorylation in the synthesis of new bis(phosphorylamino)pyridine ligands. *Mendeleev Commun.* **2010**, *20*, 223–225. [CrossRef]
42. Wang, W.-Z.; Ismayilov, R.H.; Lee, G.-H.; Liu, I.P.-C.; Yeh, C.-Y.; Peng, S.-M. The nano-scale molecule with the longest delocalized metal–metal bonds: Linear heptacobalt(II) metal string complexes $[Co_7(\mu_7\text{-}L)_4X_2]$. *Dalton Trans.* **2007**, 830–839. [CrossRef]
43. Beer, L.; Britten, J.F.; Brusso, J.L.; Cordes, A.W.; Haddon, R.C.; Itkis, M.E.; MacGregor, D.S.; Oakley, R.T.; Reed, R.W.; Robertson, C.M. Prototypal Dithiazolodithiazolyl Radicals: Synthesis, Structures, and Transport Properties. *J. Am. Chem. Soc.* **2003**, *125*, 14394–14403. [CrossRef]
44. Deacon, G.B.; Forsyth, C.M.; Scott, N.M. Structurally diverse organoamides and organoamido-, organometallic-lithium aggregates from reactions of *N*-(2-phenoxyphenyl)-*N*-(trimethylsilyl)amine with $LiBu^n$. *J. Chem. Soc. Dalton Trans.* **2001**, 2494–2501. [CrossRef]
45. Fryzuk, M.D.; Giesbrecht, G.R.; Rettig, S.J. Synthesis, Characterization, and Solution Dynamics of Alkali-Metal Chloride, Aluminate, and Borate Adducts of the Tridentate Amido Diphosphine Ligand Precursor $LiN(SiMe_2CH_2PPr^i{}_2)_2$. *Organometallics* **1997**, *16*, 725–736. [CrossRef]
46. Johnson, C.S. Diffusion ordered nuclear magnetic resonance spectroscopy: Principles and applications. *Prog. Nucl. Magn. Reson. Spectrosc.* **1999**, *34*, 203–256. [CrossRef]
47. Koehne, I.; Gerstel, M.; Bruhn, C.; Reithmaier, J.P.; Benyoucef, M.; Pietschnig, R. Azido-Functionalized Aromatic Phosphonate Esters in ^{R}POSS-Cage-Supported Lanthanide Ion (Ln = La, Nd, Dy, Er) Coordination. *Inorg. Chem.* **2021**, *60*, 5297–5309. [CrossRef] [PubMed]
48. Cabrita, E.J.; Berger, S.; Bräuer, P.; Kärger, J. High-Resolution DOSY NMR with Spins in Different Chemical Surroundings: Influence of Particle Exchange. *J. Magn. Reson.* **2002**, *157*, 124–131. [CrossRef] [PubMed]